Supplementary Information

Enabling high-performance room-temperature sodium/sulfur batteries with few-layer 2H-$MoSe_2$ embellished nitrogen-doped hollow carbon spheres as polysulfide barrier

Chunwei Dong,‡ Hongyu Zhou,‡ Bo Jin*, Wang Gao, Xingyou Lang, Jianchen Li and Qing Jiang*

Key Laboratory of Automobile Materials, Ministry of Education, School of Materials Science and Engineering, Jilin University, Changchun 130022, China

E-mail: jinbo@jlu.edu.cn; jiangq@jlu.edu.cn

‡ Chunwei Dong and Hongyu Zhou contributed equally to this work.

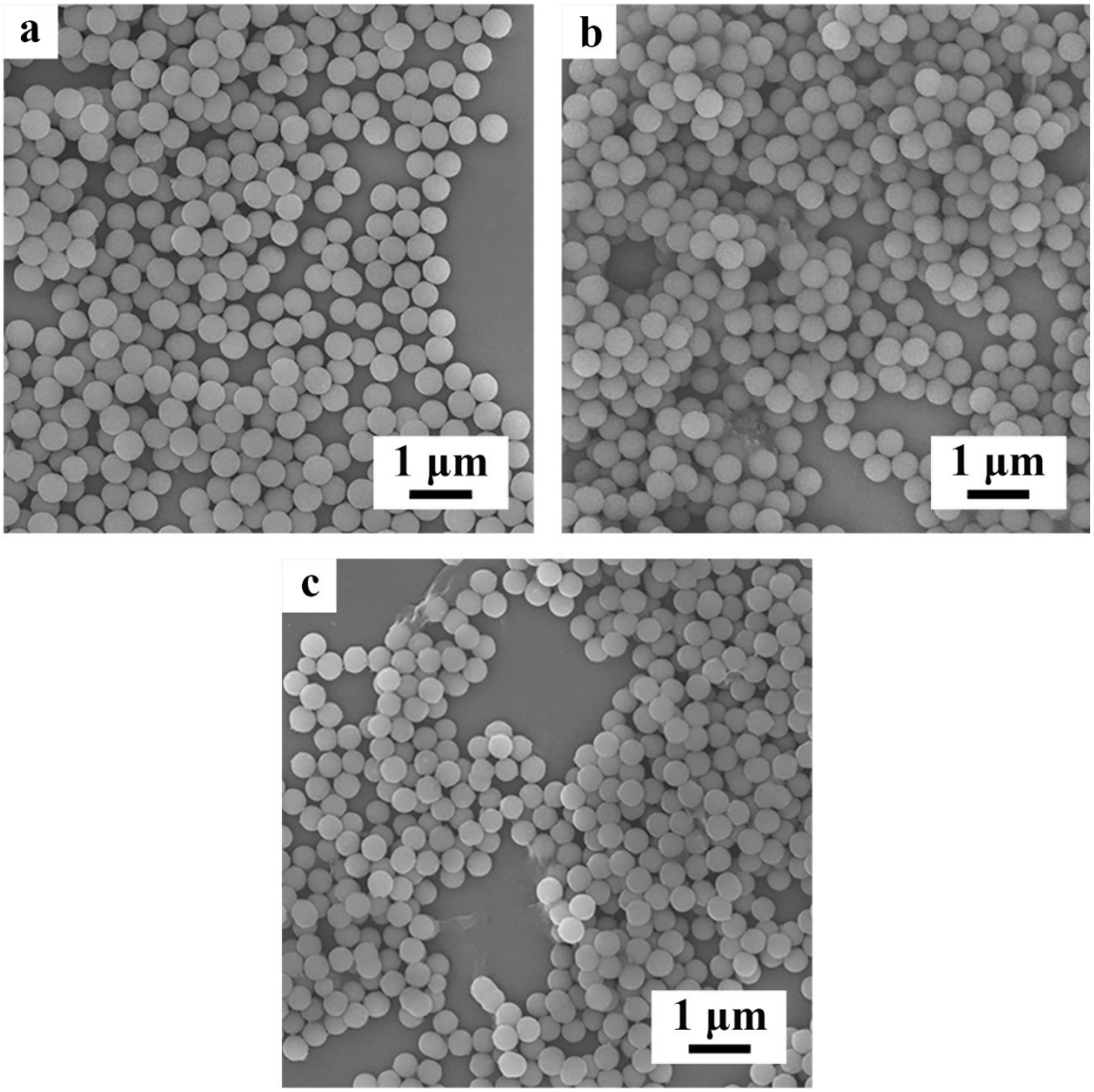

Fig. S1 Low-magnification FESEM images of (a) SiO_2, (b) SiO_2@C, and (c) N-HCS.

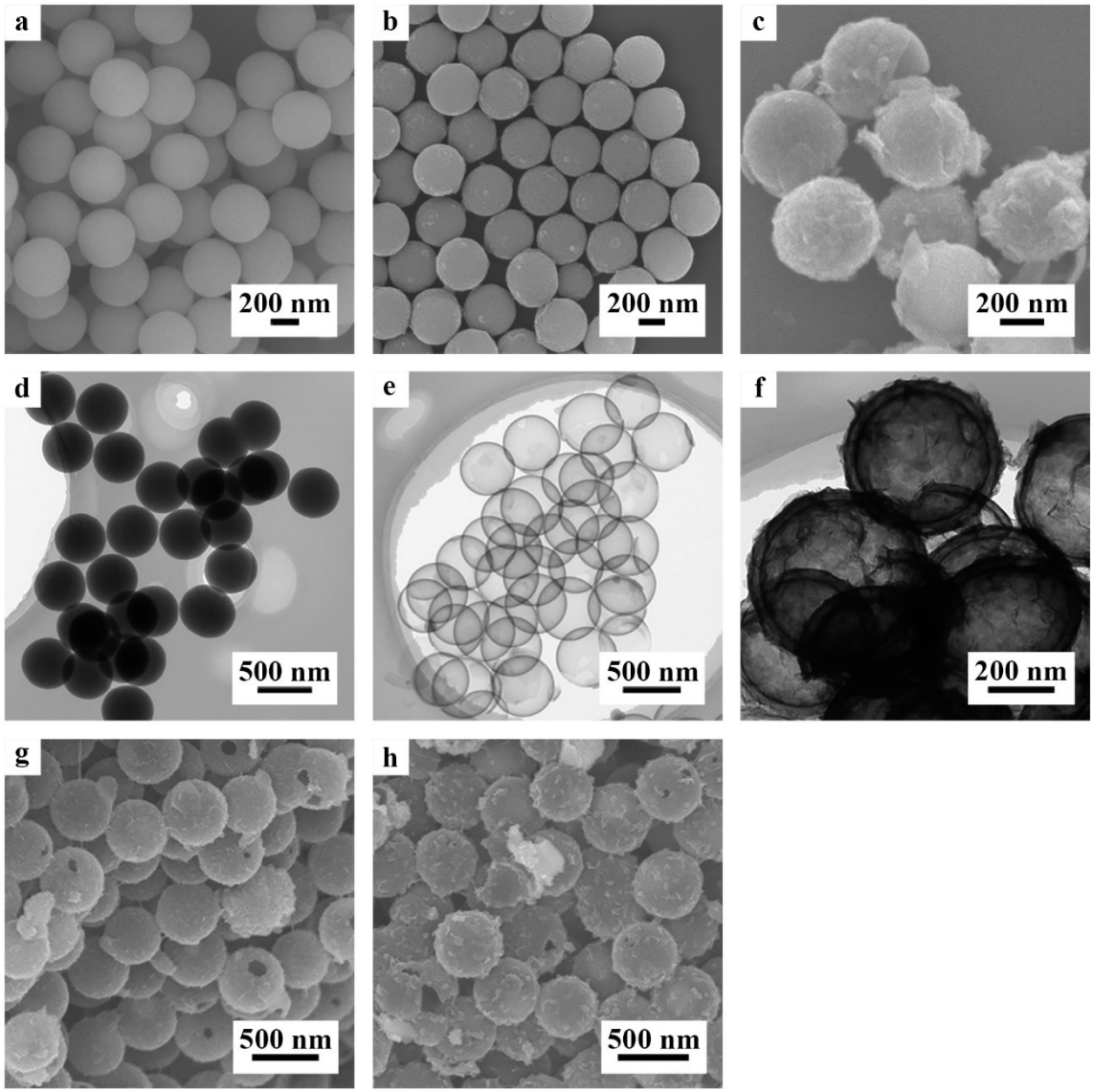

Fig. S2 (a-c) FESEM and (d-f) TEM images of SiO_2, N-HCS, and S/2H-$MoSe_2$/N-HCS. Low-magnification FESEM images of (g) 2H-$MoSe_2$/N-HCS and (h) S/2H-$MoSe_2$/N-HCS.

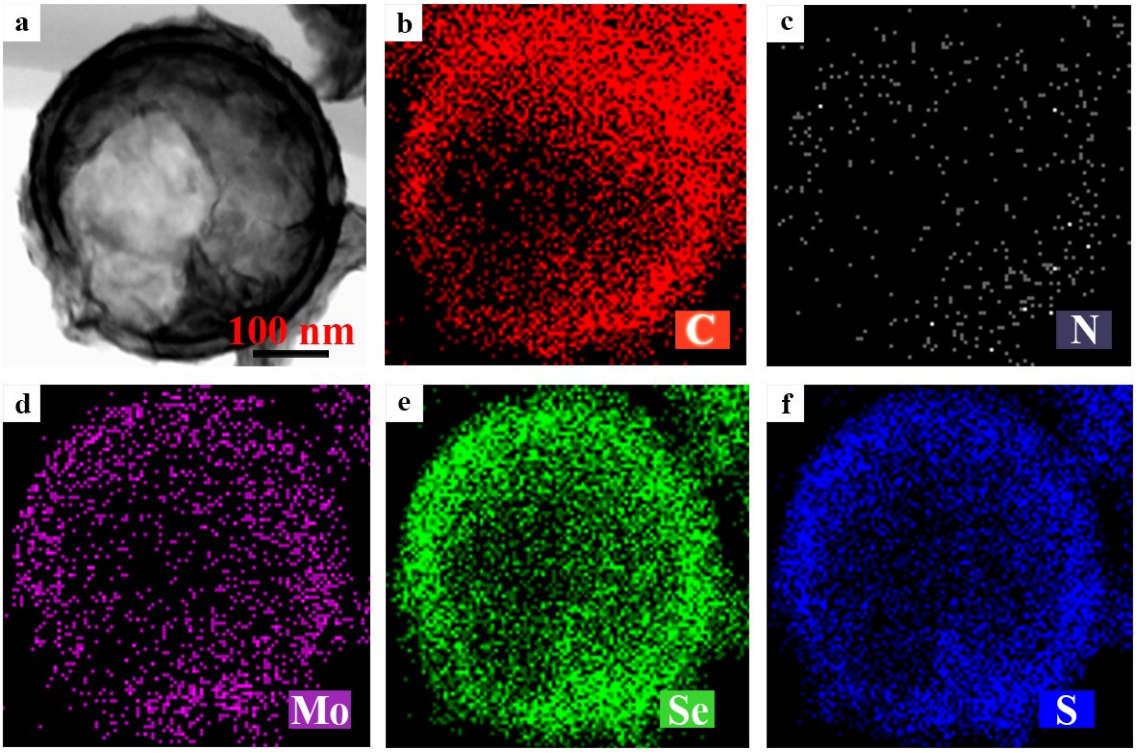

Fig. S3 (a) STEM image of S/2H-$MoSe_2$/N-HCS. (b-f) Element distribution mappings of C, N, Mo, Se, and S.

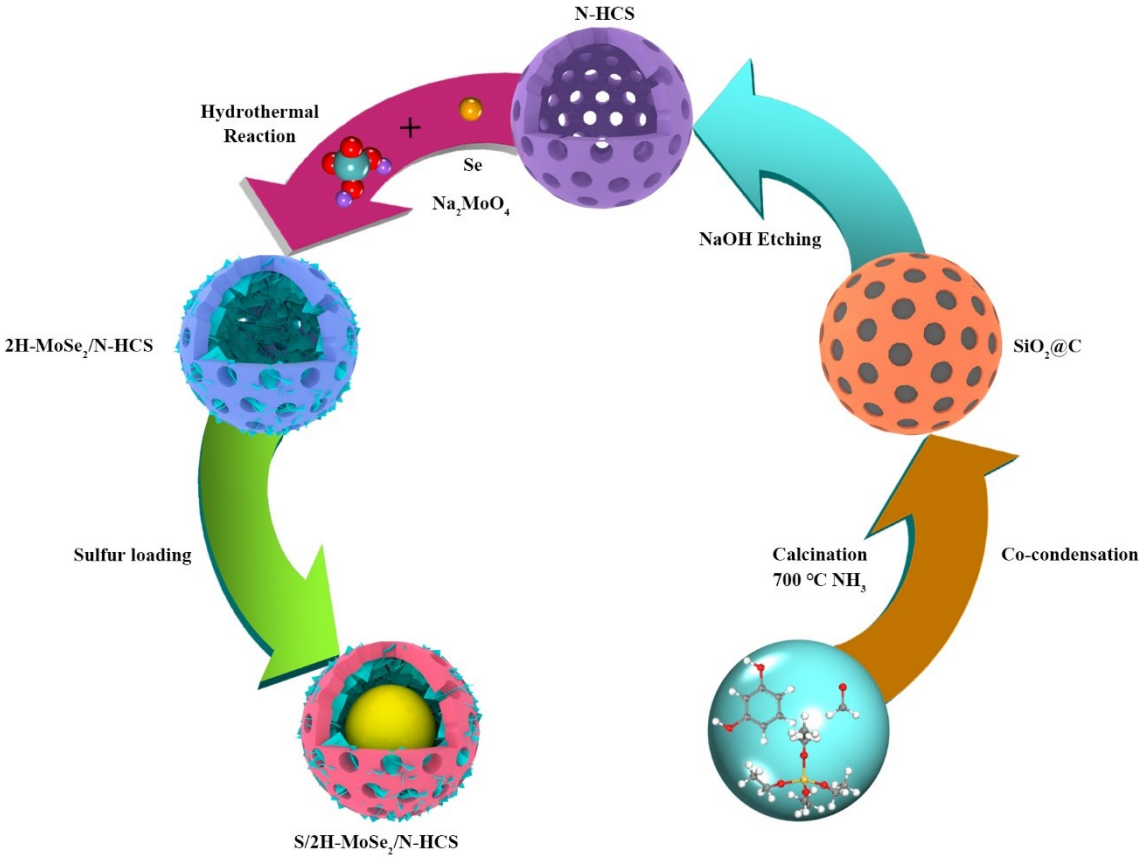

Fig. S4 Schematic illustration of fabrication process of S/2H-$MoSe_2$/N-HCS.

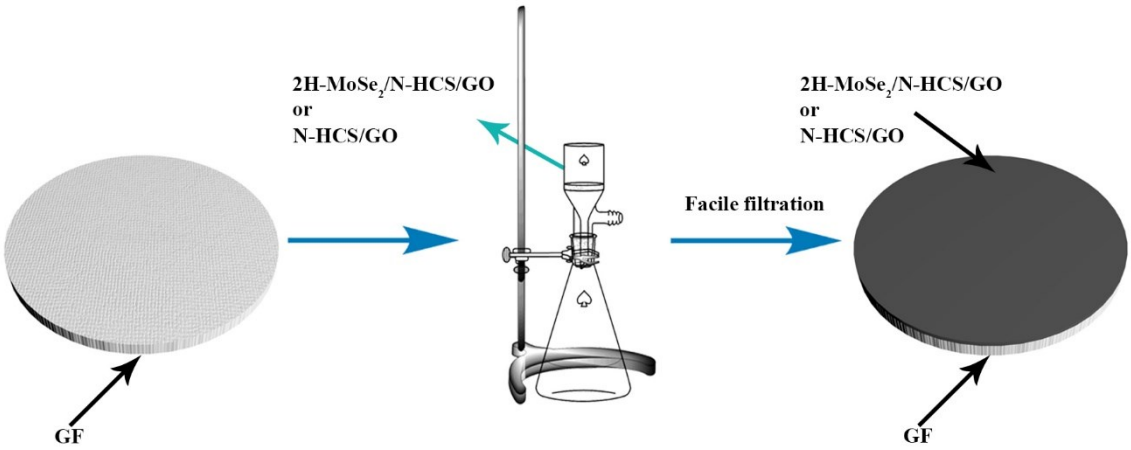

Fig. S5 Fabrication procedure of 2H-$MoSe_2$/N-HCS/GO+GF and N-HCS/GO+GF separators.

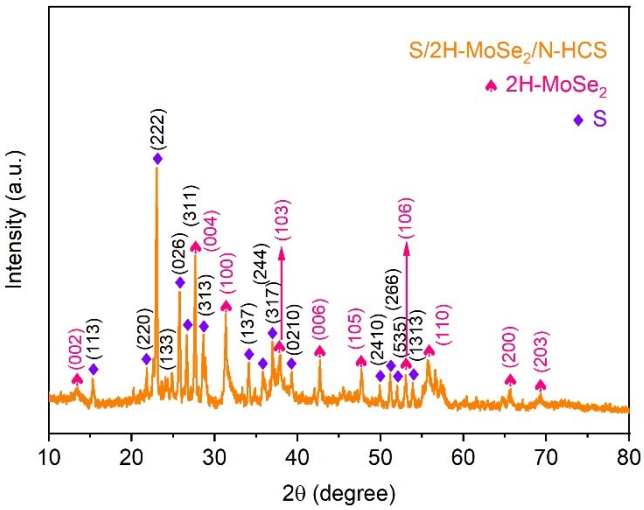

Fig. S6 XRD pattern of S/2H-$MoSe_2$/N-HCSs.

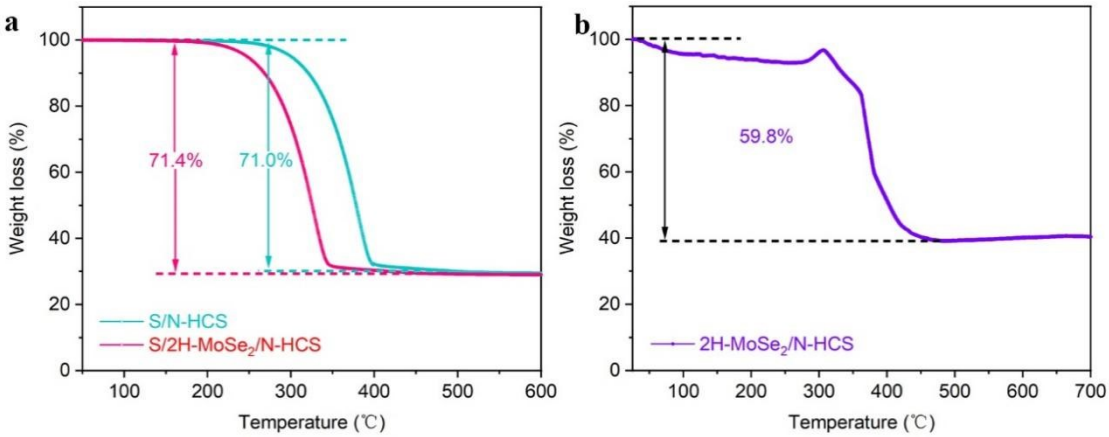

Fig. S7 (a) TGA curves of S/2H-$MoSe_2$/N-HCS and S/N-HCS. (b) TGA curve of 2H-$MoSe_2$/N-HCS. Normally, when heating, $MoSe_2$ in air produces MoO_3 and SeO_2 due to the oxidation as follows:

$2MoSe_2 + 7O_2 \rightarrow 4SeO_2 + 2MoO_3$

Afterward, the weight decreases due to the sublimation of SeO_2 and the removal of carbon by the oxidation.[1-5] The weight loss of 2H-$MoSe_2$/N-HCS is 59.8 wt%. 43.31 wt% weight loss for $MoSe_2$ is transformed into MoO_3, and 100 wt% weight loss for C is transformed into CO_2 in air.[6,7] The accurate percentage of $MoSe_2$ in 2H-$MoSe_2$/N-HCS is calculated as follows:

$M \times 59.8\% = M \times \alpha \times 43.31\% + M \times (1 - \alpha) \times 100\%$

M and α are corresponding to the weight of 2H-$MoSe_2$/N-HCS and the content of $MoSe_2$ in the composite, respectively. According to the formula, the content of $MoSe_2$ in 2H-$MoSe_2$/N-HCS is 70.6 wt%.

1 D. Xie, X. Xia, Y. Zhong, Y. Wang, D. Wang, X. Wang and J. Tu, *Adv. Energy Mater.*, 2017, **7**, 1601804.

2 M. Yousaf, Y. Wang, Y. Chen, Z. Wang, A. Firdous, Z. Ali, N. Mahmood, R. Zou, S. Guo and R. P. S. Han, *Adv. Energy Mater.*, 2019, **9**, 1900567.

3 Y. Yi, Z. Sun, C. Li, Z. Tian, C. Lu, Y. Shao, J. Li, J. Sun and Z. Liu, *Adv. Funct. Mater.*, 2020, **30**, 1903878.

4 W. Tian, B. Xi, Z. Feng, H. Li, J. Feng and S. Xiong, *Adv. Energy Mater.*, 2019, **9**, 1901896.

5 Q. Shen, P. Jiang, H. He, C. Chen, Y. Liu and M. Zhang, *Nanoscale*, 2019, **11**, 13511-13520.

6 Z. Luo, J. Zhou, L. Wang, G. Fang, A. Pan and S. Liang, *J. Mater. Chem. A*, 2016, **4**, 15302-15308.

7 Y. Wu, M. Xu, X. Chen, S. Yang, H. Wu, J. Pan and X. Xiong, *Nanoscale*, 2016, **8**, 440-450.

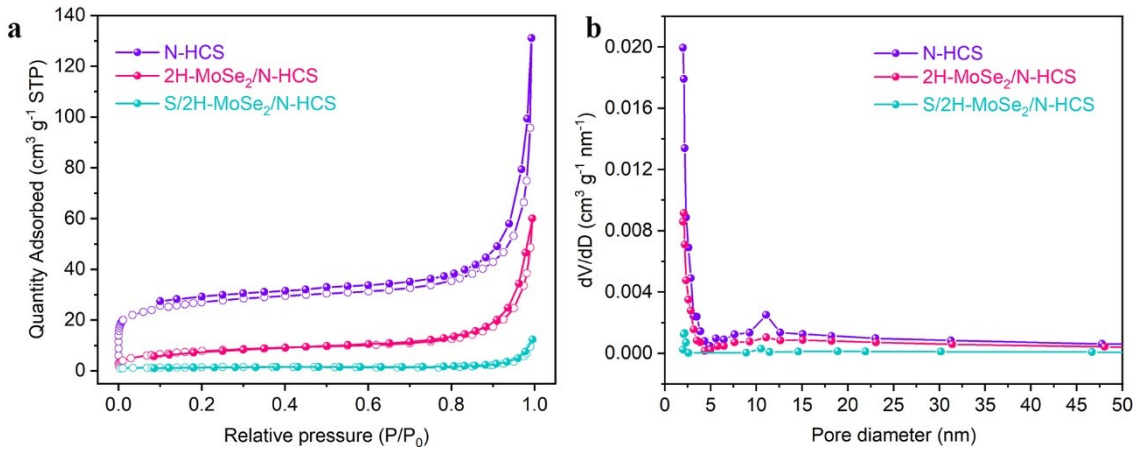

Fig. S8 (a) N_2 adsorption-desorption isotherms and (b) pore size analysis of N-HCS, 2H-$MoSe_2$/N-HCS, and S/2H-$MoSe_2$/N-HCS.

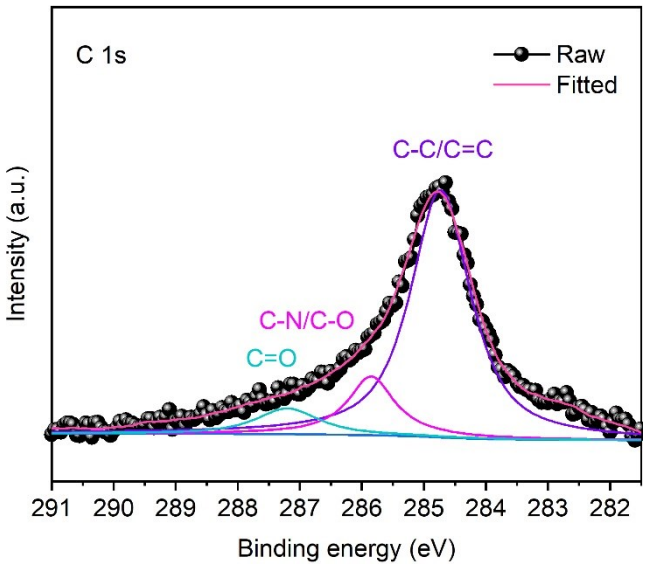

Fig. S9 High-resolution XPS plot of C 1s in 2H-$MoSe_2$/N-HCS.

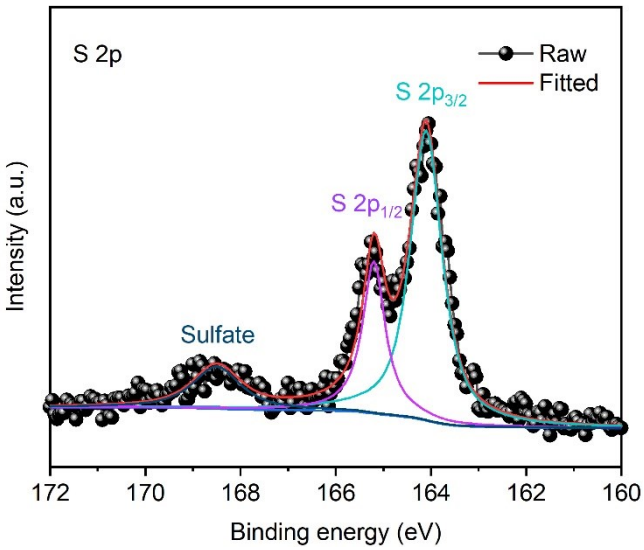

Fig. S10 High-resolution XPS plot of S 2p in S/2H-$MoSe_2$/N-HCS before cycling.

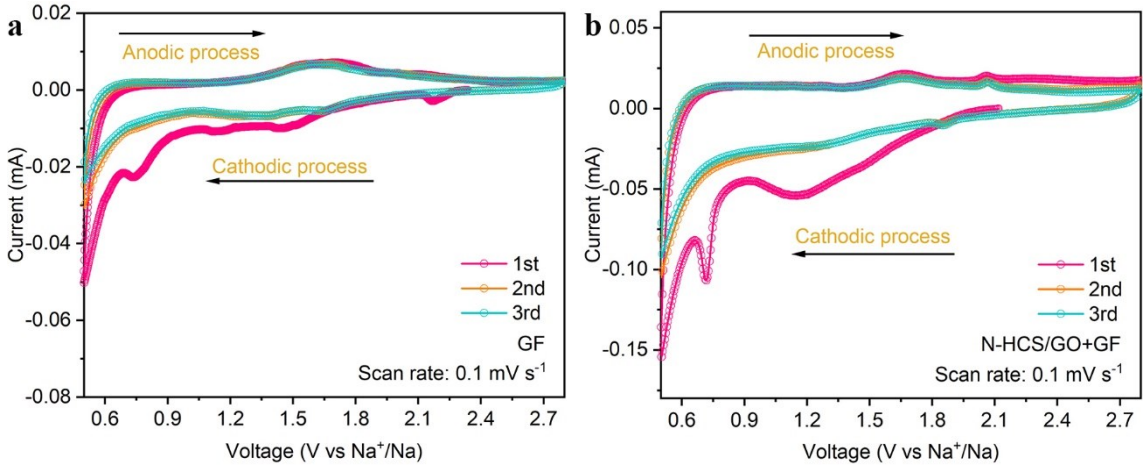

Fig. S11 CV curves of RT-Na/S batteries with (a) pristine GF and (b) N-HCS/GO+GF separators at the voltage range of 0.5 to 2.8 V (vs Na^+/Na) and scan rate of 0.1 mV s^{-1}.

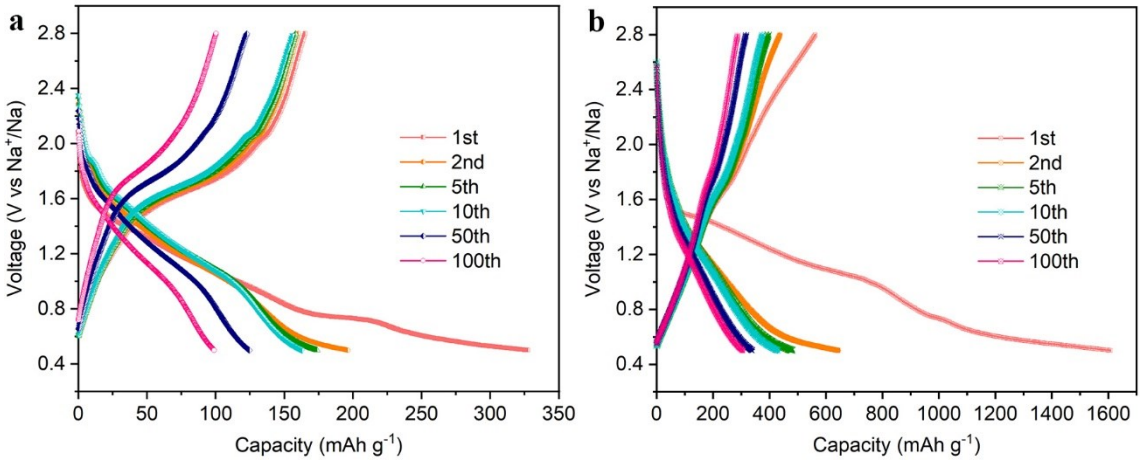

Fig. S12 Charge/discharge profiles of RT-Na/S batteries with (a) pristine GF and (b) N-HCS/GO+GF separators at 0.1 C.

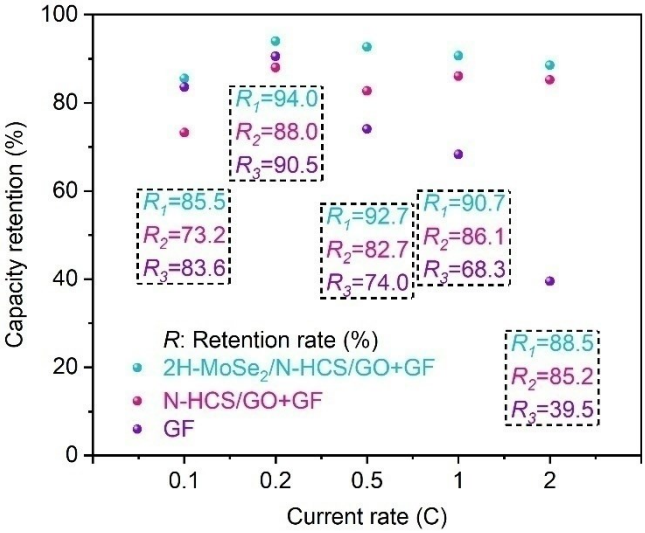

Fig. S13 Capacity retention of RT-Na/S batteries with different separators at different current rates.

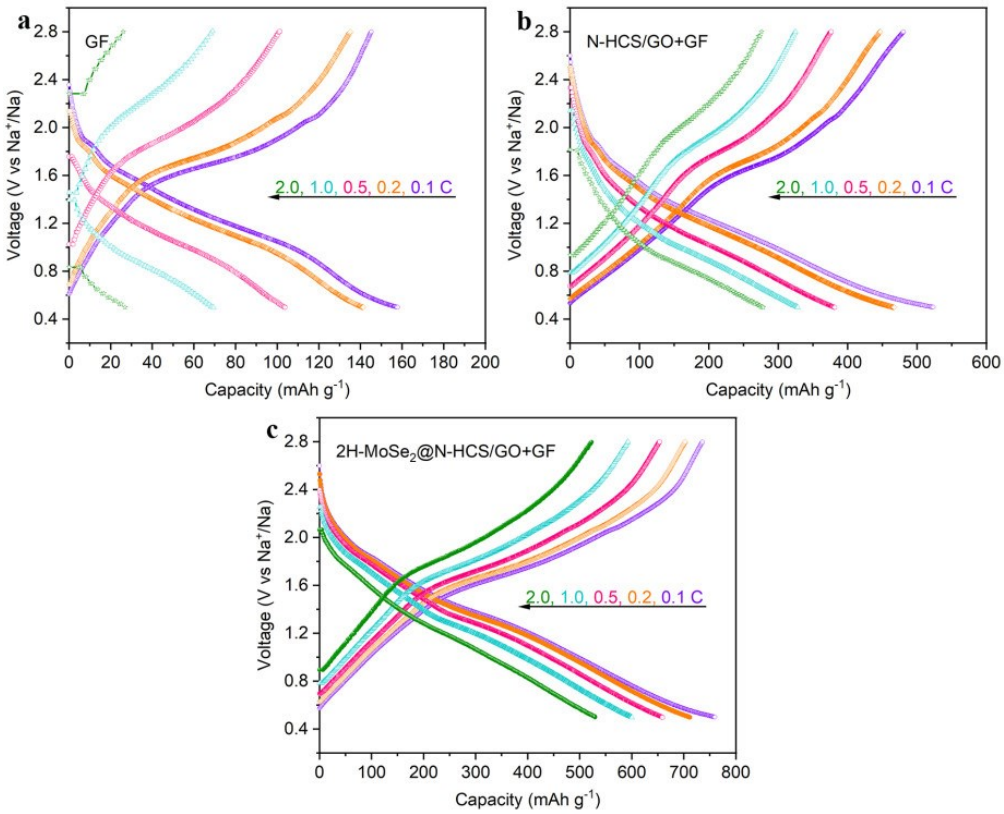

Fig. S14 Charge/discharge curves of RT-Na/S batteries with pristine (a) GF, (b) N-HCS/GO+GF, and (c) 2H-$MoSe_2$/N-HCS/GO+GF separators at various current rates.

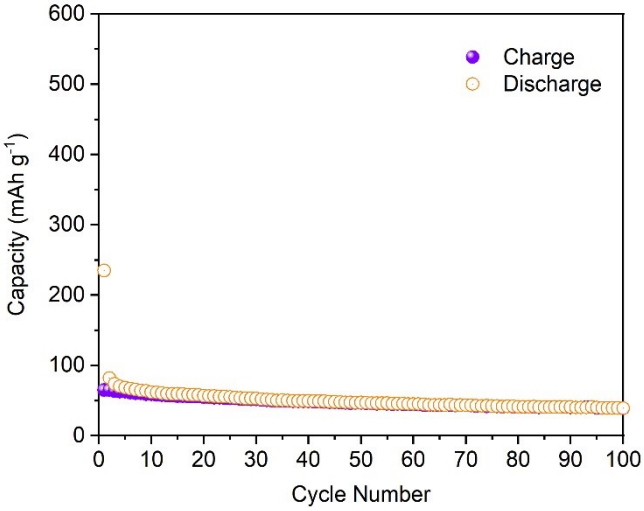

Fig. S15 Cycling performance of $MoSe_2$ electrode at a current density of 0.5 C.

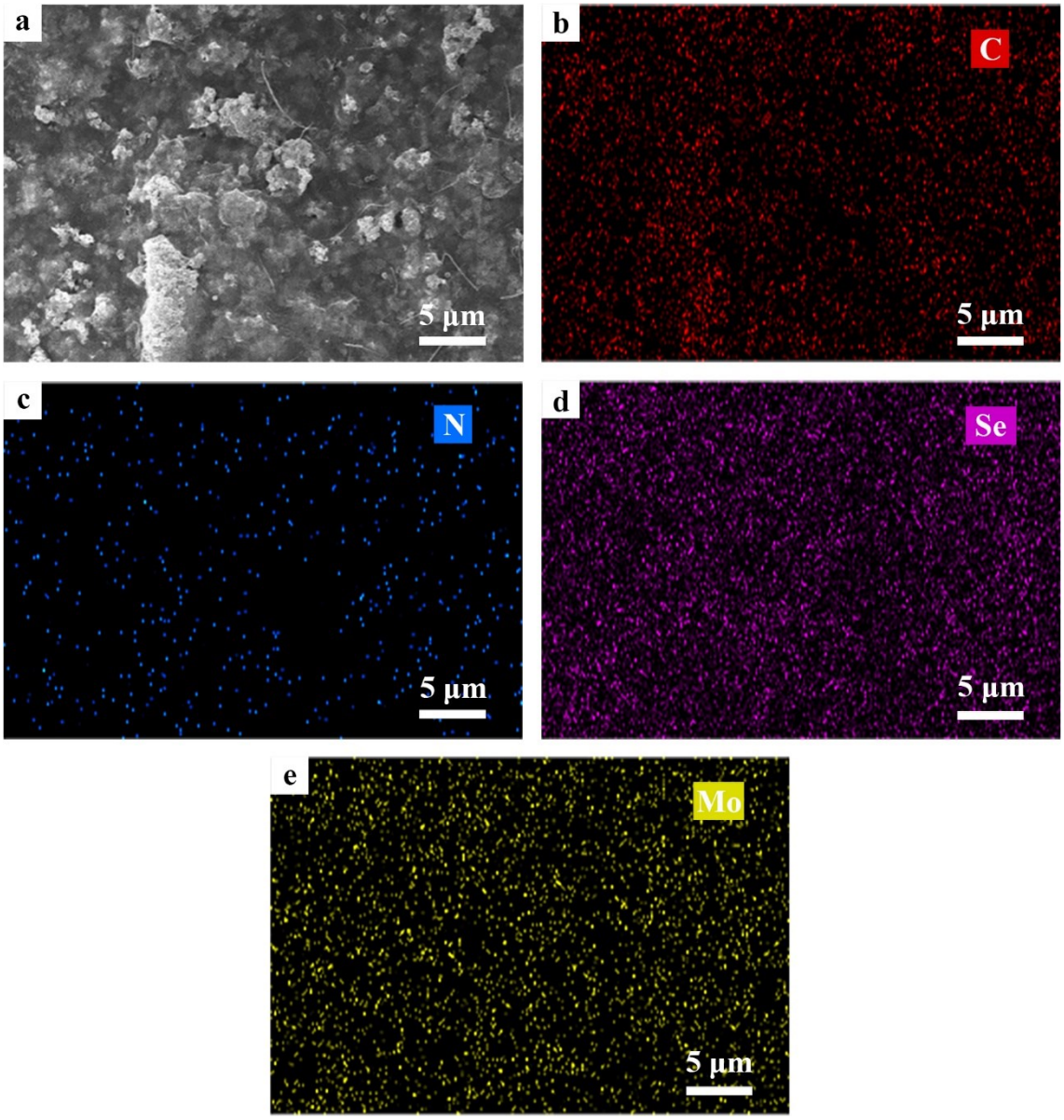

Fig. S16 (a) Low-magnification SEM image of 2H-$MoSe_2$/N-HCS/GO+GF separator. The corresponding elemental mappings in a selected region before cycling: (b) C, (c) N, (d) Se, and (e) Mo.

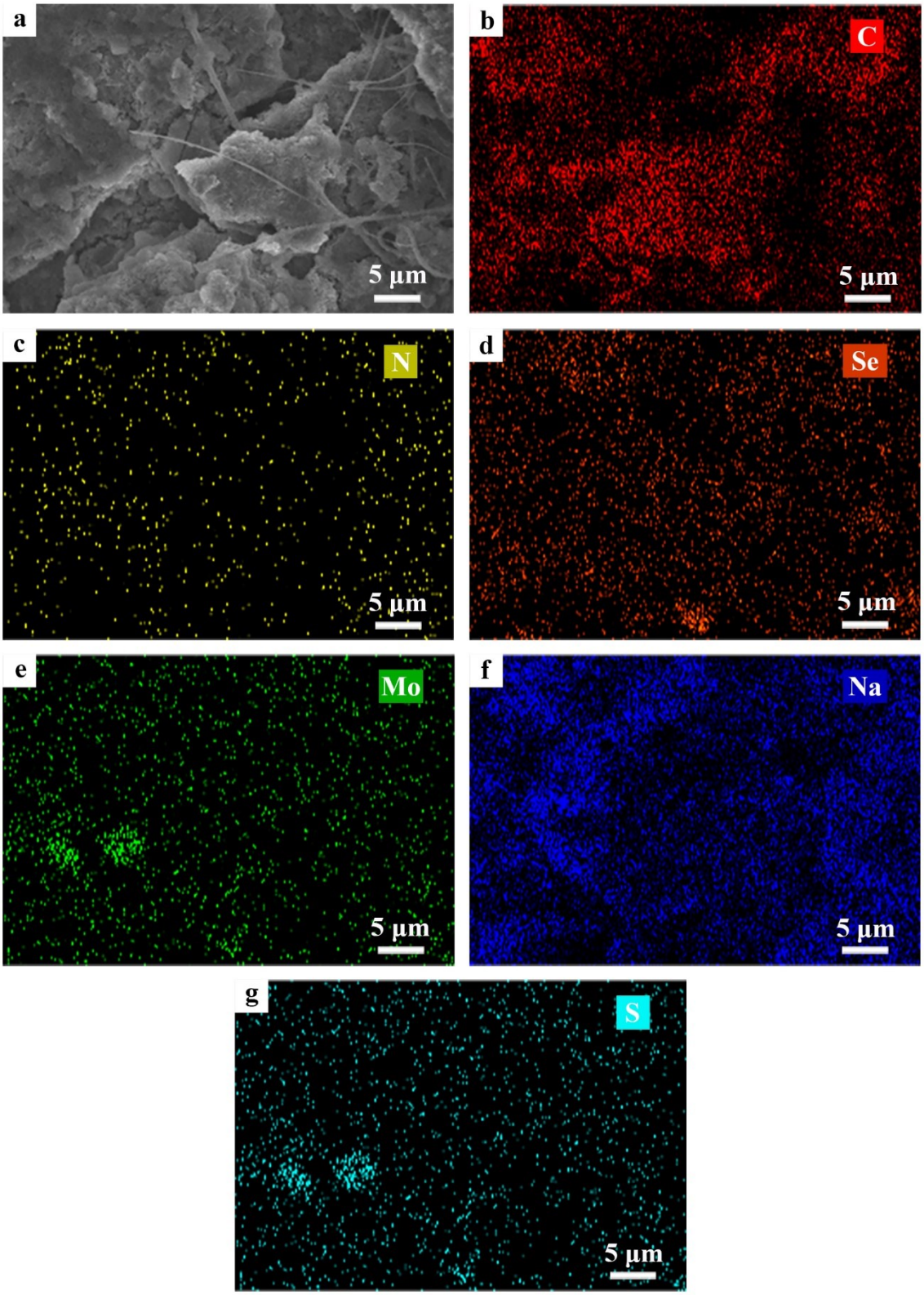

Fig. S17 (a) Low-magnification SEM image of 2H-$MoSe_2$/N-HCS/GO+GF separator after cycling. The corresponding elemental mappings: (b) C, (c) N, (d) Se, (e) Mo, (f) Na, and (g) S.

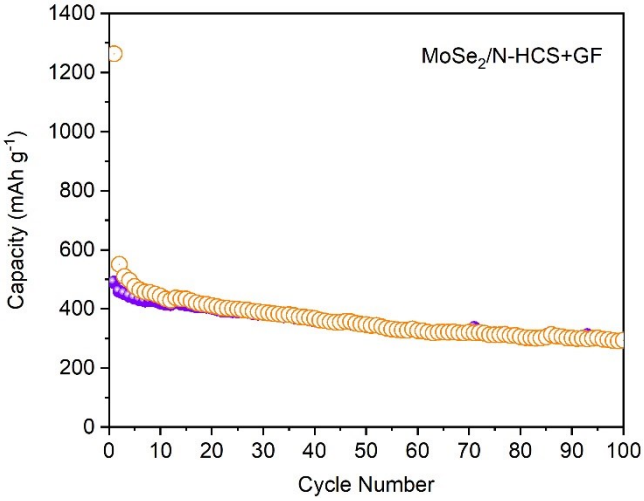

Fig. S18 Cycling performance of a RT-Na/S battery with a 2H-$MoSe_2$/N-HCS+GF separator at a current density of 0.5 C.

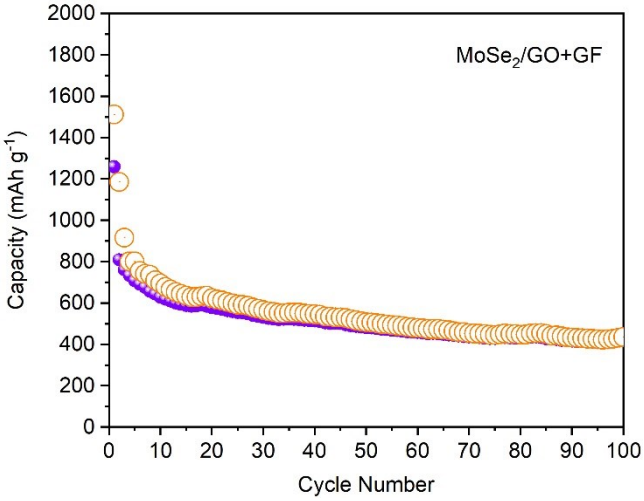

Fig. S19 Cycling performance of a RT-Na/S battery with a $MoSe_2$/GO+GF separator at a current density of 0.5 C.

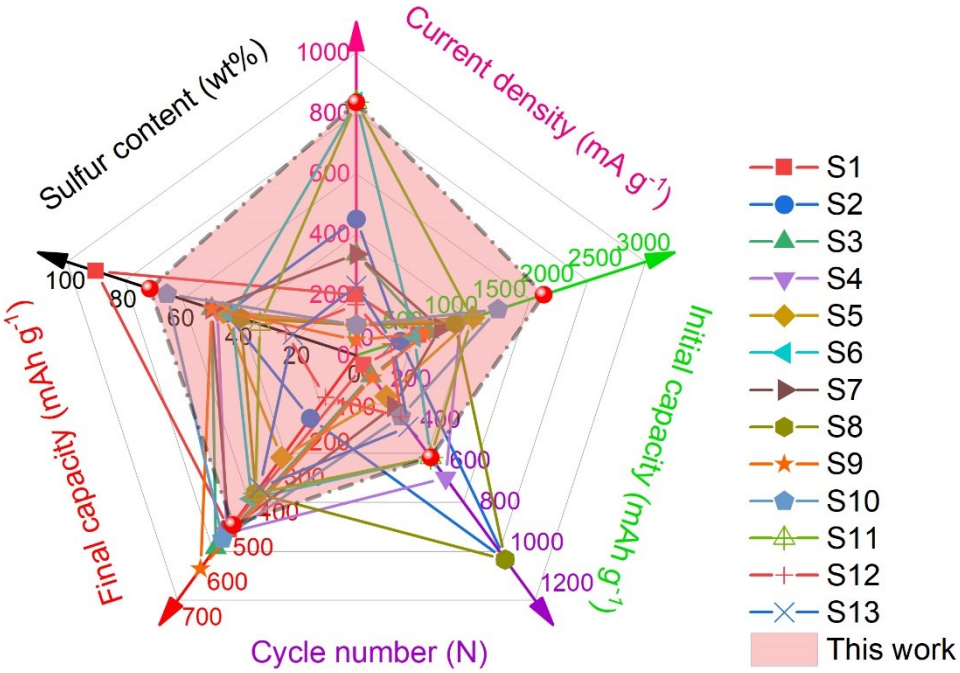

Fig. S20 Comparison of the electrochemical performance of RT-Na/S batteries with other reported literatures.

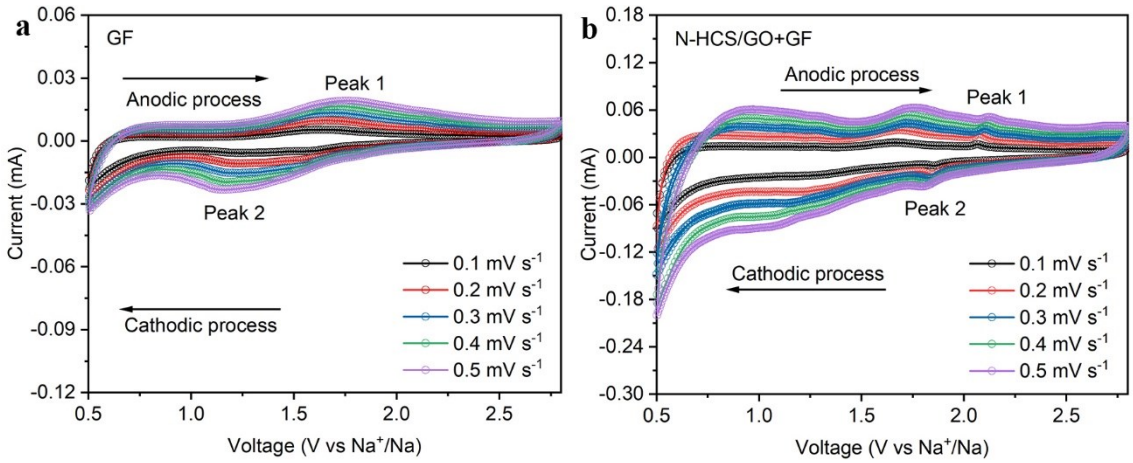

Fig. S21 CV curves of RT-Na/S batteries with (a) pristine GF and (b) N-HCS/GO+GF separators at different scan rates from 0.1 to 0.5 mV s^{-1}.

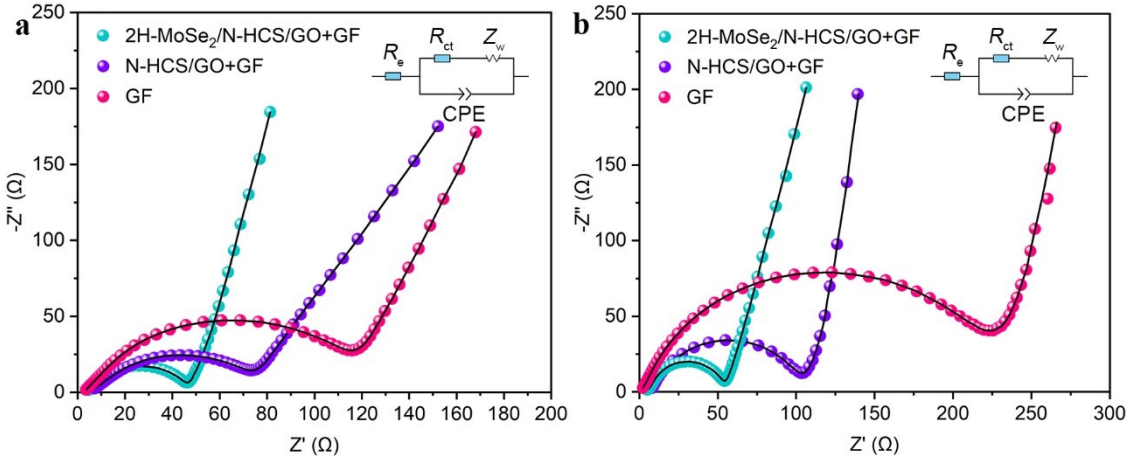

Fig. S22 Nyquist plots of RT-Na/S batteries with different separators (a) before cycling and (b) after ten cycles at 0.1 C (insets: the equivalent electrical circuits).

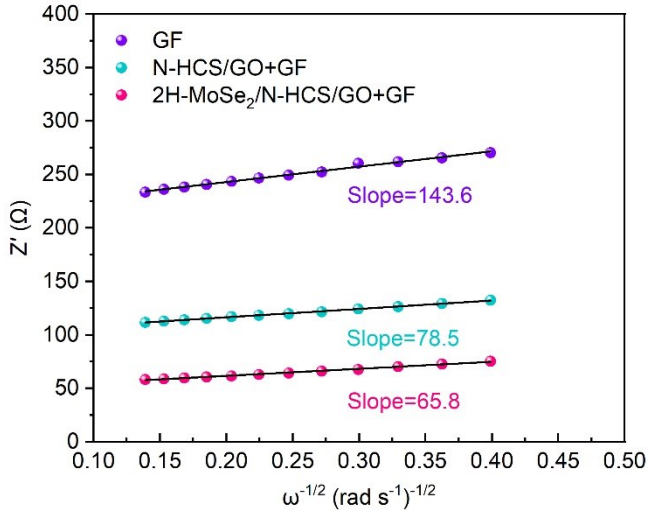

Fig. S23 The relationship plots of RT-Na/S batteries with different separators after cycles between Z′ and $\omega^{-1/2}$ in the low-frequency region.

The electrochemical impedance spectroscopy was further generalized to analyze the solid-state ion diffusion behaviors by using Nyquist plots in the low-frequency region (Fig. S22b). Na-ion diffusion coefficient was calculated by the following equation:[1-3]

$$D_{Na^+} = R^2 T^2/2A^2 n^4 F^4 C_{Na}^2 \sigma_\omega^2 \quad (1)$$

Where R is the gas constant, T represents the absolute temperature, A is the area of electrode, n is the number of the transferred electrons, F is the Faraday constant, and C_{Na} is the concentration of sodium-ion. Besides, σ_ω is Warburg coefficient, which is determined as the slope of Z′ versus $\omega^{-1/2}$ (Fig. S23) in the low-frequency region based on the following equation:

$$Z' = R_e + R_{ct} + \sigma_\omega \omega^{-1/2} \quad (2)$$

Where ω is the angular frequency, R_e is the resistance of electrolyte, and R_{ct} is the charge transfer resistance. Na-ion diffusion coefficients of RT-Na/S batteries with GF, N-HCS/GO+GF, and 2H-$MoSe_2$/N-HCS/GO+GF separators are 5.98×10^{-14}, 2.0×10^{-13}, and 2.84×10^{-13} cm^2 s^{-1}, respectively. D_{Na^+} of a RT-Na/S battery with 2H-$MoSe_2$/N-HCS/GO+GF separator is higher than those of the other two RT-Na/S batteries with N-HCS/GO+GF and GF separators, indicating its improved rate capability (Fig. 4d).

1 A. J. Bard and L. R. Faulkner, Electrochemical Methods, Second Ed., Wiley, 2001, 231.

2 J. Mou, T. Liu, Y. Li, W. Zhang, M. Li, Y. Xu, J. Huang and M. Liu, *J. Mater. Chem. A*, 2020, **8**, 24590-24597.

3 P. Ge, H. Hou, S. Li, L. Yang and X. Ji, *Adv. Funct. Mater.*, 2018, **28**, 1801765.

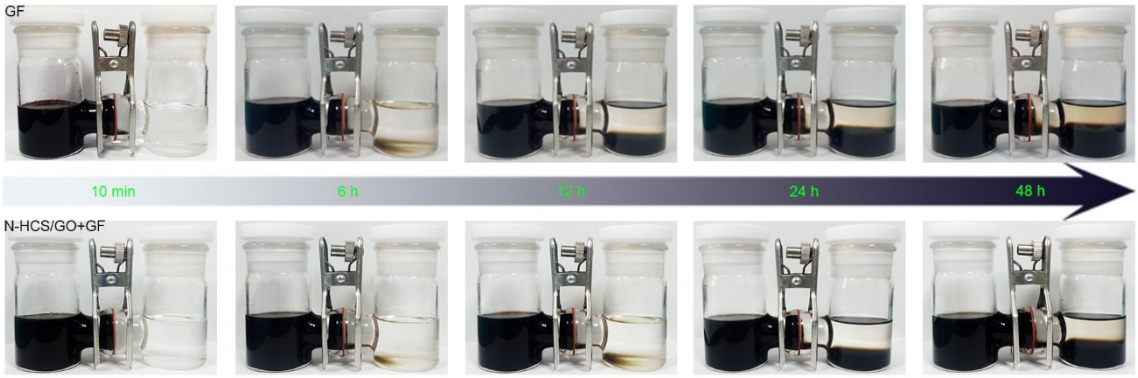

Fig. S24 SPSs permeation measurements in H-type cells with the pristine GF and N-HCS/GO+GF separators after different time.

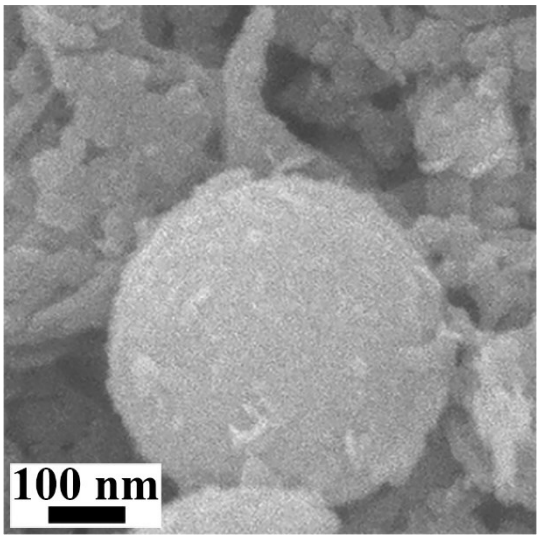

Fig. S25 High-magnification SEM image of S/2H-$MoSe_2$/N-HCS after cycles.

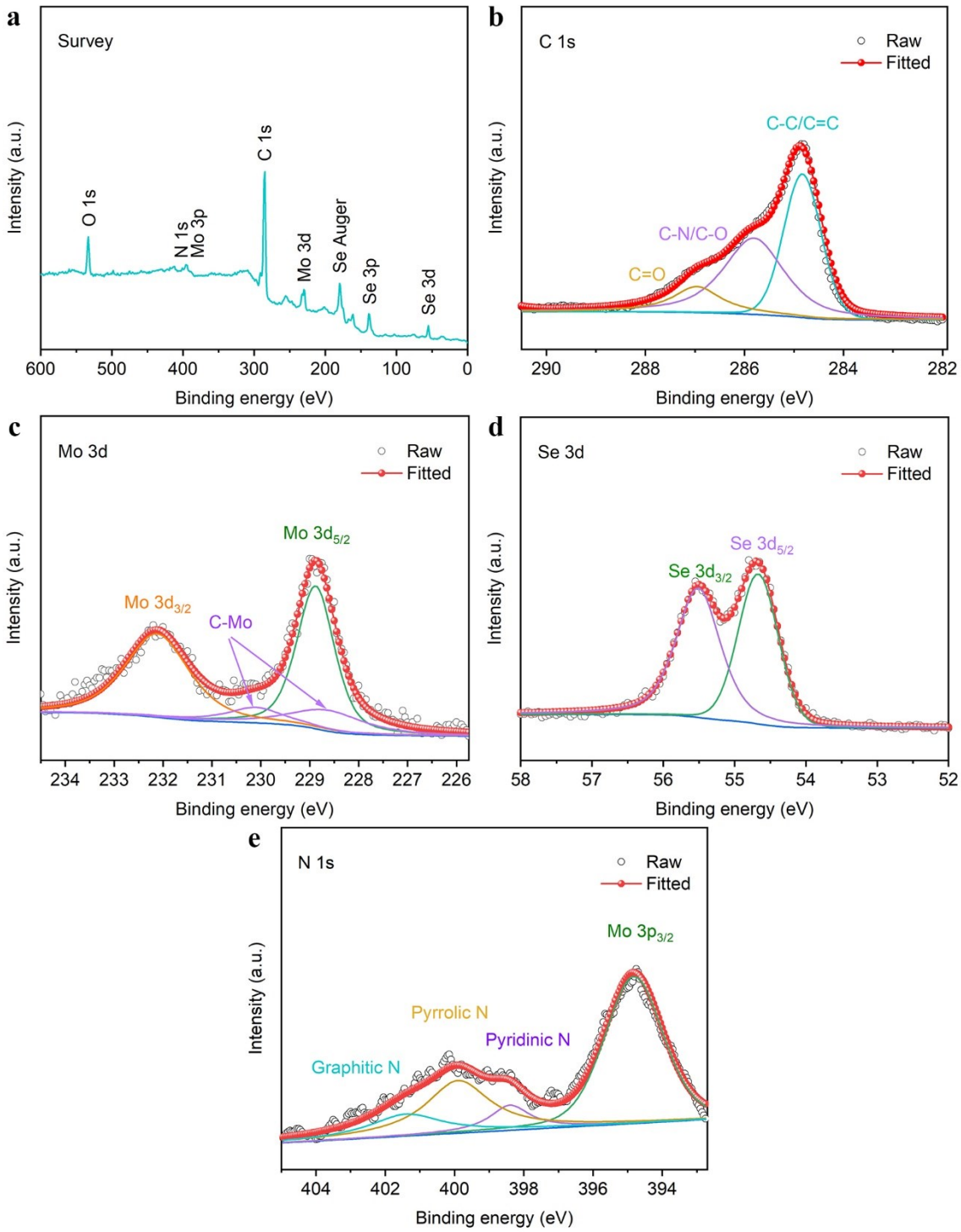

Fig. S26 (a) XPS survey spectrum, (b) C 1s, (c) Mo 3d, (d) Se 3d, and (e) N 1s high-resolution XPS spectra of S/2H-$MoSe_2$/N-HCS after cycles.

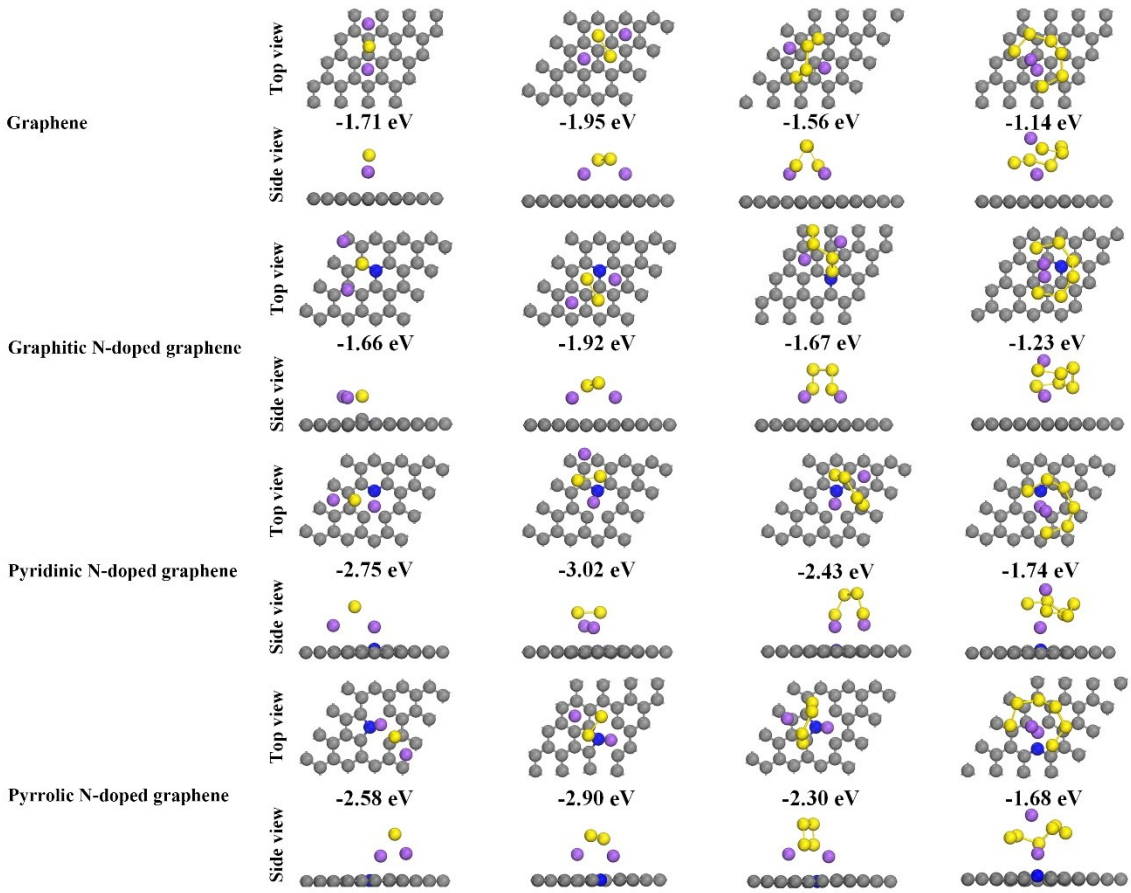

Fig. S27 The optimized configurations and corresponding adsorption energies for binding of Na_2S, Na_2S_2, Na_2S_4, and Na_2S_6 to graphene and N-doped graphene.

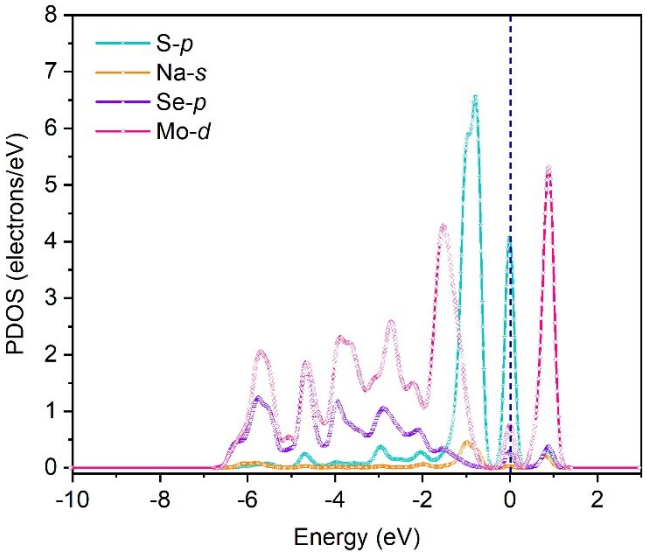

Fig. S28 Partial density of states (PDOS) of Na_2S adsorbed on $MoSe_2$, including Na-*s*, S-*p*, Se-*p*, and Mo-*d* orbitals.

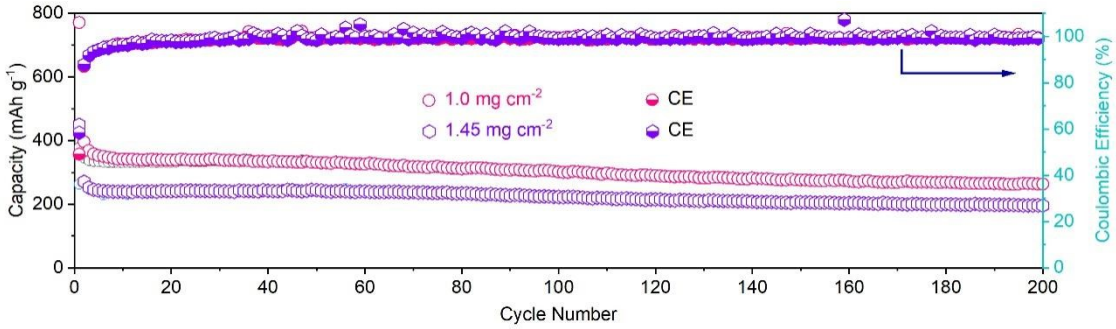

Fig. S29 Cycling performance of RT-Na/S batteries with 2H-$MoSe_2$/N-HCS/GO+GF separator at high sulfur loadings at 0.5 C.

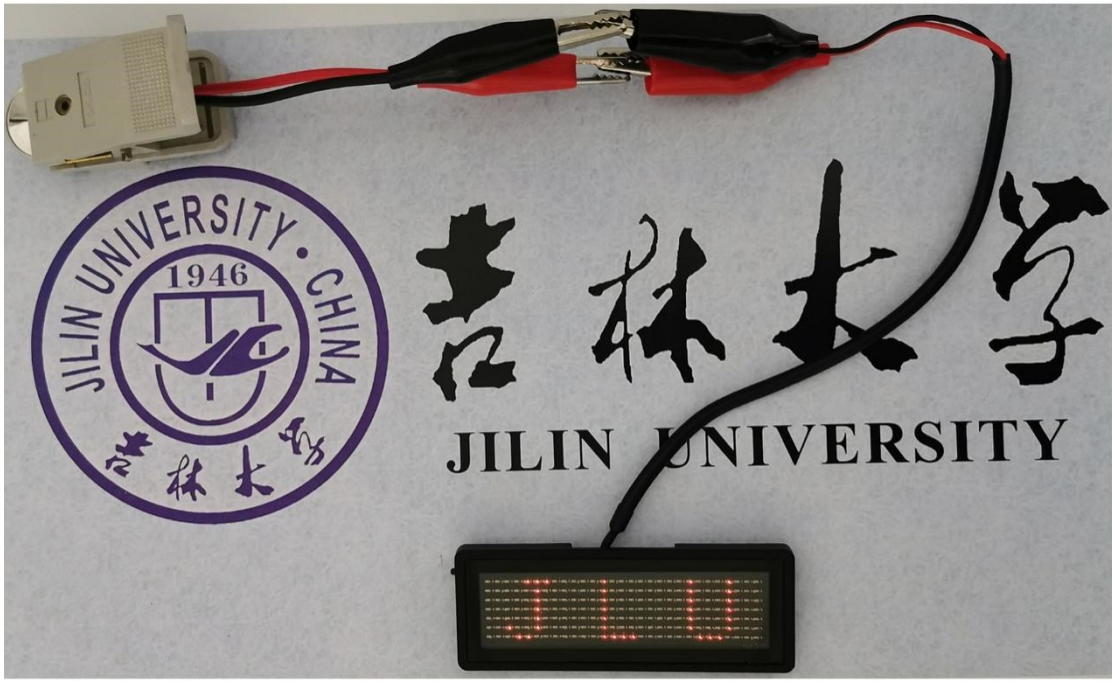

Fig. S30 Photograph of a LED array panel with a “JLU” pattern lighted by a RT-Na/S battery with a 2H-$MoSe_2$/N-HCS/GO+GF separator.

Table S1 Comparison of the electrochemical performance between this work and other recently reported literatures for RT-Na/S batteries.

Cathode material	Current density (mA g^{-1})	Initial capacity (mAh g^{-1})	Final capacity (mAh g^{-1})	Cycle number (N)	Sulfur content (wt%)	Ref.
CS90-rGO	200	650	498	50	~90	S1
MoS_3	450	460	~180	1000	45	S2
CNF/AC-Na_2S_6	335	750	550	100	50	S3
S@Co_n-HC	100	1081	508	600	48	S4
S@iMCHS	100	1215	292	200	46	S5
S@CNT/NPC	837.5	601	410	500	43	S6
cZIF-8/S	335	873	500	250	50	S7
S@Fe-HC	100	1023	394	1000	40	S8
HSMC-Cu-S	50	710	610	110	50	S9
FeS_2@NCMS/S	100	1471	524	300	65.5	S10
Microporous carbon/sulfur	837.5	1200	395	500	33.4	S11
CFC/S-2	167.5	360	120	300	24.4	S12
N, S-HPC/S	230	381	378	350	22	S13
S/2H-$MoSe_2$/N-HCS	**837.5**	**1945**	**484**	**500**	**71.4**	**This work**

*Results summarized from Fig. S20 in Supporting Information.

References

S1 Ghosh, S. Shukla, M. Monisha, A. Kumar, B. Lochab and S. Mitra, *ACS Energy Lett.*, 2017, **2**, 2478-2485.

S2 H. L. Ye, L. Ma, Y. Zhou, L. Wang, N. Han, F. P. Zhao, J. Deng, T. P. Wu, Y. G. Li and J. Lu, *PNAS*, 2017, **114**, 13091-13096.

S3 X. W. Yu and A. Manthiram, *Adv. Energy Mater.*, 2015, **5**, 1500350.

S4 B. W. Zhang, T. Sheng, Y. D. Liu, Y. X. Wang, L. Zhang, W. H. Lai, L. Wang, J. P. Yang, Q. F. Gu, S. L. Chou, H. K. Liu and S. X. Dou, *Nat. Commun.*, 2018, **9**, 4082.

S5 Y. X. Wang, J. P. Yang, W. H. Lai, S. L. Chou, Q. F. Gu, H. K. Liu, D. Y. Zhao and S. X. Dou, *J. Am. Chem. Soc.*, 2016, **138**, 16576-16579.

S6 T. T. Yang, W. Gao, B. S. Guo, R. M. Zhan, Q. J. Xu, H. He, S. J. Bao, X. Y. Li, Y. M. Chen and M. W. Xu, *J. Mater. Chem. A*, 2019, **7**, 150-156.

S7 Y. M. Chen, W. F. Liang, S. Li, F. Zou, S. M. Bhaway, Z. Qiang, M. Gao, B. D. Vogt and Y. Zhu, *J. Mater. Chem. A*, 2016, **4**, 12471-12478.

S8 B. W. Zhang, T. Sheng, Y. X. Wang, S. L. Chou, K. Davey, S. X. Dou and S. Z. Qiao, *Angew. Chem.*, 2019, **131**, 1498-1502.

S9 S. Y. Zheng, P. Han, Z. Han, P. Li, H. J. Zhang and J. H. Yang, *Adv. Energy Mater.*, 2014, **4**, 1400226.

S10 Z. C. Yan, Y. R. Liang, J. Xiao, W. H. Lai, W. L. Wang, Q. B. Xia, Y. X. Wang, Q. F. Gu, H. M. Lu, S. L. Chou, Y. Liu, H. K. Liu and S. X. Dou, *Adv. Mater.*, 2020, **32**, 1906700.

S11 V. Kumar, A. Y. S. Eng, Y. Wang, D. T. Nguyen, M. F. Ng and Z. W. Seh, *Energy Storage Mater.*, 2020, **29**, 1-8.

S12 Q. Q. Lu, X. Y. Wang, J. Cao, C. Chen, K. N. Chen, Z. F Zhao, Z. Q. Niu and J. Chen, *Energy Storage Mater.*, 2017, **8**, 77-84.

S13 Z. Qiang, Y. M. Chen, Y. F. Xia, W. F. Liang, Y. Zhu and B. D. Vogt, *Nano Energy*, 2017, **32**, 59-66.

Table S2 The values of R_{ct} of RT-Na/S batteries with different separators before cycling and after cycles.

Separator	**R_{ct} (Ω) Before cycling**	**R_{ct} (Ω) After ten cycles**
2H-$MoSe_2$/N-HCS/GO+GF	41.32	49.25
N-HCS/GO+GF	66.51	95.97
GF	112.41	221.32